

To be appeared in ApJ, 617, 20 December 2004 issue

Starburst at the Expanding Molecular Superbubble in M82: Self-Induced Starburst at the Inner Edge of the Superbubble

Satoki Matsushita¹

Harvard-Smithsonian Center for Astrophysics, 60 Garden St., MS-78, Cambridge, MA 02138

smatsushita@cfa.harvard.edu

Ryohei Kawabe

National Astronomical Observatory of Japan, 2-21-1 Osawa, Mitaka, Tokyo 181-8588, Japan

Kotaro Kohno

Institute of Astronomy, University of Tokyo, 2-21-1 Osawa, Mitaka, Tokyo 181-0015, Japan

Hironori Matsumoto and Takeshi G. Tsuru

Department of Physics, Faculty of Science, Kyoto University, Sakyo-ku, Kyoto 606-8502, Japan

and

Baltasar Vila-Vilaró

Steward Observatory, University of Arizona, Tucson, AZ 85721

ABSTRACT

We present high spatial resolution ($2''.3 \times 1''.9$ or $43 \text{ pc} \times 36 \text{ pc}$ at $D = 3.9 \text{ Mpc}$) 100 GHz millimeter-wave continuum emission observations with the Nobeyama Millimeter Array toward an expanding molecular superbubble in the central region of M82. The 100 GHz continuum image, which is dominated by free-free

¹Present address: Academia Sinica, Institute of Astronomy and Astrophysics, P.O. Box 23-141, Taipei 106, Taiwan, R.O.C.; satoki@asiaa.sinica.edu.tw

emission, revealed that the four strongest peaks are concentrated at the inner edge of the superbubble along the galactic disk. The production rates of Lyman continuum photons calculated from 100 GHz continuum flux at these peaks are an order of magnitude higher than those from the most massive star forming regions in our Galaxy. At these regions, high velocity ionized gas (traced by H41 α and [Ne II]) can be seen, and H₂O and OH masers are also concentrated. The center of the superbubble, on the other hand, is weak in molecular and free-free emissions and strong in diffuse hard X-ray emission. These observations suggest that a strong starburst produced energetic explosions and resultant plasma and superbubble expansions, and induced the present starburst regions traced by our 100 GHz continuum observations at the inner edge of the molecular superbubble. These results, therefore, provide the first clear evidence of self-induced starburst in external galaxies. Starburst at the center of the superbubble, on the other hand, begins to cease because of a lack of molecular gas. This kind of intense starburst seems to have occurred several times within $10^6 - 10^7$ years in the central region of M82.

Subject headings: galaxies: individual (M82, NGC 3034) — galaxies: ISM — galaxies: starburst — ISM: bubbles — radio lines: galaxies

1. INTRODUCTION

Messier 82 (NGC 3034, Cigar Galaxy) is known as one of the nearby (3.9 Mpc; Sakai & Madore 1999), bright irregular galaxies, and, therefore, has been studied by many authors, at many wavelengths, and over many years. Optical observations (Lynds & Sandage 1963; Shopbell & Bland-Hawthorn 1998; Ohyama et al. 2002) show remarkable features of kpc-scale filaments extending above and below the disk of this galaxy. Soft X-ray (Watson, Stanger, & Griffiths 1984; Kronberg, Biermann, & Schwab 1985; Bregman, Schulman, & Tomisaka 1995; Tsuru et al. 1997; Strickland, Ponman, & Stevens 1997), molecular gas (Nakai et al. 1987; Matsushita et al. 2000; Taylor, Walter, & Yun 2001; Walter, Weiss, & Scoville 2002), and dust (Kuno & Matsuo 1997; Alton, Davies, & Bianchi 1999) observations also show filamentary structures outside the disk region. These observations suggest that the filamentary structures are the result of explosions, which occurred within the nuclear region. The mass-to-luminosity ratio, M/L , of this galaxy is extremely low (< 0.02 , Rieke & Lebofsky 1979; ≈ 0.04 , Telesco 1993) as compared with normal galaxies (5 – 10, Rieke & Lebofsky 1978) and can be explained by bursts of star formation or a starburst (Rieke & Lebofsky 1978; Rieke et al. 1980).

The starburst in M82 is believed to be triggered by a tidal interaction with the nearby two-armed spiral galaxy M81. Neutral hydrogen (H I) emission observation toward the M81 group shows that there is a tidal bridge between M81 and M82, suggesting that there is a close encounter between these two galaxies $\sim 10^8$ years ago (e.g., Cottrell 1977; Yun, Ho, & Lo 1994). Optical and near-infrared imaging and spectroscopic observations toward the disk region (0.5 – 1 kpc outside from the galactic center) of M82 indicate that the starburst occurred at this region $\sim 10^8$ years ago, corresponds to the episode of the tidal interaction with M81 (O’Connell & Mangano 1978; Gallagher & Smith 1999; de Grijs, O’Connell, & Gallagher 2001; Smith & Gallagher 2001). Since the present starburst region is located at the center, they suggested that the global starburst in M82 has propagated inward from the disk to the nuclear regions. The evolution of starburst at the nuclear 500 pc region is, on the other hand, still unclear. Some authors suggest the nuclear starburst propagated outward (e.g., Satyapal et al. 1995, 1997; Förster Schreiber et al. 2003), and some inward (e.g., Shen & Lo 1995).

Interferometric molecular gas observations show an arc-like deviation from rigid rotation in position-velocity (PV) diagrams at ~ 140 pc westward from the galactic nucleus, and this deviation implies the existence of an expanding molecular superbubble (Neininger et al. 1998; Weiss et al. 1999; Wills et al. 1999). The existence of the superbubble was confirmed by imaging the shell-like structure with the size of 260 pc \times 170 pc (Matsushita et al. 2000; Wills, Pedler, & Muxlow 2002). The age and the total energy of the superbubble are estimated to be about $(1 - 2) \times 10^6$ yr and $\sim (0.5 - 2) \times 10^{55}$ ergs, which corresponds to the total energy of $\sim 10^3 - 10^4$ supernovae. At the center of the superbubble, there is a “2.2 μ m secondary peak” (a primary peak corresponds to the nucleus; Dietz et al. 1986; Lester et al. 1990), which is dominated by luminous supergiants (Joy, Lester, & Harvey 1987). Since luminous supergiants are the late phase of OB stars, it is reasonable to suppose that a starburst has occurred at this near-infrared peak in the recent past. Actually, calculations of the initial mass function of this peak suggest that the number of supernovae, which have already exploded within the age of the superbubble, can explain the total energy of the superbubble. It is therefore concluded that this superbubble has been produced as a result of localized starburst at the “2.2 μ m secondary peak” (Matsushita et al. 2000).

Detailed information about the nature of starburst in this region is, however, still not clear, because the central region of M82 is deeply obscured by dust even in the K-band (e.g., $A_K \sim 1.4$, McLeod et al. 1993; $A_K \sim 1.0$, Satyapal et al. 1995; $A_K \lesssim 0.8$, Telesco et al. 1991: These correspond to $A_V \sim 14$, ~ 10 , and $\lesssim 8$, respectively, if we assume $A_V/A_K = 10$; Draine 1989). Hence it is very hard to derive detailed information — such as the precise flux of recombination lines — in the optical or near-infrared.

On the other hand, 100 GHz continuum observations are generally dominated by the free-free emission and would not be affected by the dust absorption, as is the case for optical or near-infrared observations. In fact, spectral energy distribution (SED) studies from the infrared to radio wavelength region of M82 indicates that the 100 GHz continuum emission in M82 is dominated by free-free emission (Condon 1992; Matsuo et al. 1998). A detailed SED study for small-scale structures toward the central region of M82 by Carlstrom & Kromberg (1991) based on their millimeter and centimeter interferometric (BIMA and VLA) observations concluded that the free-free emission dominates even in the small-scale structures of 100 GHz continuum emission (i.e., 100 GHz continuum emission from all the peaks are dominated by free-free emission). Hence, 100 GHz continuum observations can have great advantages for the observation of the central starburst regions in M82, where a large amount of dust exists.

In this paper, we report the structures and properties of the present starburst regions and environment in M82 with our high spatial resolution 100 GHz observations and compare them with previously published data. We also discuss the triggering of new starbursts by the past energetic starburst and the resultant superbubble expansion, namely, self-induced starburst.

2. OBSERVATIONS

We obtained aperture synthesis 100 GHz continuum images toward the central region of M82 with the Nobeyama Millimeter Array during 1997 December – 1998 April. Three (AB, C, and D) configurations of six 10 m antennas, equipped with tunerless SIS receivers (Sunada, Kawabe, & Inatani 1994), were used for the observations. As back-end, we used an XF-type spectro-correlator Ultra Wide Band Correlator (UWBC; Okumura et al. 2000b), which has a 1 GHz bandwidth and a 6 GHz intermediate frequency. Since the UWBC can process both the upper side band (USB) and the lower side band (LSB), our continuum data were obtained from the USB of the HCN(1 – 0) observations (the rest frequency of the HCN $J = 1 - 0$ line is 88.632 GHz, and the observed frequency is 88.884 GHz). Hence the central frequency of the continuum observations corresponds to 100.884 GHz. The band-pass calibration was done with 3C273, and 0923+392 was observed every 10 minutes as a phase and amplitude calibrator. The flux scale of 0923+392 was determined by comparisons with Mars and Uranus. The uncertainty in the absolute flux scale is estimated to be $\sim 20\%$.

The data were reduced using the NRO software package “UVPROC II” (Tsutsumi, Morita, & Umeyama 1997), and the final maps were made and CLEANed with the NRAO software AIPS. We analyzed the 100 GHz continuum data with uniform uv weighting at the

CLEAN process, and the resultant resolution was $2''.3 \times 1''.9$ (43 pc \times 36 pc at $D = 3.9$ Mpc). We note that this linear scale of the beam size is similar to the typical diameter of a giant molecular cloud (GMC).

3. RESULTS

3.1. Distribution of 100 GHz Continuum Emission

The 100 GHz continuum map made with uniform *uv* weighting is shown in Figure 1. We defined a “peak” as (1) detected in the map with 6σ or more and (2) separated from other peaks by more than one beam width. We found seven peaks in the map (Peaks A–G in the figure), and all peaks were aligned along the galactic disk (position angle or P.A. of 76°). The four strongest peaks, D–G, correspond to the two strongest peaks in the previously published lower spatial resolution 100 GHz continuum images (Carlstrom & Kromberg 1991; Brouillet & Schilke 1993; Seaquist et al. 1996; Neininger et al. 1998). Other weaker peaks in our map correspond to those in the previously published images. Note that our lower resolution ($3''.7 \times 3''.3$) and higher signal-to-noise ratio map (i.e., natural *uv* weighting map; not shown in this paper) is consistent with other published results.

Since the uniform *uv* weighting increases the noise level of the map, the diffuse extended emission may be masked by the noise, and the total flux of the 100 GHz continuum emission may decrease compared with the natural *uv* weighting image. However, the total flux of the uniform *uv* weighting map is, in fact, $\sim 80\%$ of that of the natural *uv* weighting map, which suggests that most of the flux is not missing. On the other hand, the total flux of our natural *uv* weighting map is 0.43 Jy, and the missing flux compared with the single-dish flux (~ 0.54 Jy; Jura, Hobbs, & Maran 1978) is $\sim 20\%$, which is almost comparable with the uncertainty in the absolute flux scale. We therefore did not recover the missing flux and conclude that the high spatial resolution starburst properties, as reported here, are accurate at the 30% level.

Figure 2 shows the $^{12}\text{CO}(1 - 0)$ superbubble image (contour map; Matsushita et al. 2000) overlaid on the 100 GHz continuum image (colorscape map). The dashed line shows the possible oval structure of the superbubble. This figure shows that *the four brightest peaks (D-G) in the 100 GHz continuum image are located at the inner edge of the molecular superbubble along the galactic disk of M82*. We also made an 100 GHz continuum intensity plot of the superbubble sliced along the major axis (P.A. = 76°), namely along the galactic disk, of the galaxy to compare with that of the ^{12}CO emission (Fig. 3). The continuum emission has a double-peaked structure in the plot: The intensity is weak at the center of

the superbubble (around zero offset in the figure) and has peaks at both sides of the bubble center, which are located around $\pm(2'' - 4'')$ offsets. The plot of the ^{12}CO emission also shows a double-peaked structure. The emission is weak at the center of the bubble, but peaks are located around $\pm(4'' - 7'')$, outside the peaks of the continuum emission. This figure demonstrates that the 100 GHz emission is located at the inner edge of the molecular superbubble.

Since the 100 GHz continuum emission in M82 is dominated by free-free emission, even in small-scale structures (see §1), these 100 GHz continuum emitting regions represent starburst regions. This distribution, therefore, strongly suggests that the present starburst regions in M82 are concentrated at the inner edge of the molecular superbubble.

3.2. Production Rates of Lyman Continuum Photons

The 100 GHz continuum emission in M82 is dominated by free-free emission, as mentioned above, so that the strength of the emission is directly related to star formation activities like $\text{H}\alpha$ emission at optical wavelength. Furthermore, 100 GHz continuum emission does not be affected by the dust absorption like the $\text{H}\alpha$ emission. Figure 4 shows the $\text{H}\alpha$ image (colroscale map; Ohyama et al. 2002) overlaid on the 100 GHz continuum image (contour map). The map clearly shows that the brightest 100 GHz continuum peaks are totally obscured by dust in the $\text{H}\alpha$ image, indicating that 100 GHz continuum observation is a strong tool to image the active starburst regions directly.

We therefore use the 100 GHz continuum emission flux (i.e., absorption-free free-free emission flux), S_{T} , to estimate the production rates of Lyman continuum photons, N_{Ly} . The absorption-free N_{Ly} can be calculated as

$$\left(\frac{N_{\text{Ly}}}{[\text{s}^{-1}]} \right) \sim 1.8 \times 10^{51} \left(\frac{T_{\text{e}}}{10^4 \text{ [K]}} \right)^{-0.45} \left(\frac{\nu}{100.88 \text{ [GHz]}} \right)^{0.1} \left(\frac{D}{3.9 \text{ [Mpc]}} \right)^2 \left(\frac{S_{\text{T}}}{[\text{mJy}]} \right), \quad (1)$$

where T_{e} and ν are the electron temperature and the observation frequency, respectively (Rubin 1968; Condon 1992). We adopted $D = 3.9$ Mpc (Sakai & Madore 1999) for the distance of M82. Since radio recombination line observations toward the central region of M82 suggest that T_{e} of the ionized gas (different from hot plasma which can be seen in X-ray emission) ranges between $\sim 5,000$ K and $\sim 10,000$ K (Seaquist et al. 1996; Seaquist, Kerton, & Bell 1994; Puxley et al. 1989), we used $T_{\text{e}} = 5,000$ K and 10,000 K for the calculations.

We substitute the peak flux density of the 100 GHz continuum averaged over the beam size of $2''.3 \times 1''.9$ (43 pc \times 36 pc) into eq. (1), and derived N_{Ly} at the specific regions (Peaks A-G in Fig. 1) in M82 (Table 1). We find that N_{Ly} in the present star forming regions

averaged over the linear scale of about $30 - 40$ pc are as high as $\sim (3 - 6) \times 10^{52}$ photons s^{-1} for the four strong peaks (D–G; the western side of the nucleus) and $\sim (2 - 3) \times 10^{52}$ photons s^{-1} for other weaker peaks (the eastern side of the nucleus). The uncertainty of N_{Ly} is about $(0.4 - 0.5) \times 10^{52}$ photons s^{-1} , which corresponds to 1σ statistical uncertainty in the continuum map.

To find out the validity of our estimation of N_{Ly} , we compared our estimation with those of infrared observations. Förster Schreiber et al. (2001) estimated $2''.25 \times 2''.25$ aperture size N_{Ly} using their $Br\gamma$ image, which is corrected for extinction of $A_V \sim 45 \pm 20$. The N_{Ly} at their position B2, which corresponds to our Peak D, is $(3.24 \pm 1.33) \times 10^{52}$ photons s^{-1} , consistent with that of Peak D of $(4.2 - 5.7) \times 10^{52}$ photons s^{-1} (Table 1). Satyapal et al. (1997) also estimated N_{Ly} using their $Br\gamma$ image, corrected for reddening of about $A_V \sim 10$. They found 12 point-like sources at the central 500 pc region using an extinction corrected K-band image, and calculated for N_{Ly} with $2''$ aperture size, similar to our beam size. N_{Ly} values for the eastern side of the nucleus show $\sim (0.3 - 0.8) \times 10^{52}$, and those of western side show $\sim (0.8 - 1.4) \times 10^{52}$. The tendency that N_{Ly} of the western side is about twice as strong as that of the eastern side is the same as our results. Their absolute values are, however, a factor of a few smaller than our estimation and that of Förster Schreiber et al. (2001). This inconsistency maybe due to their smaller reddening correction. In summary, our N_{Ly} estimation using 100 GHz continuum flux and that using infrared emission line data are consistent each other.

4. DISCUSSION

In the previous section, we show that the present starburst regions are strongly concentrated at the inner edge of the expanding molecular superbubble. In this section, we discuss the starburst activities, environment, and history around the superbubble.

4.1. Comparison of Star Formation Activity with Our Galaxy and Nearby Galaxies

Since the linear scale of our beam size is comparable to those of GMCs, it is worth comparing the star forming activity around the superbubble in M82 with those in active star forming GMCs in our Galaxy and nearby galaxies using N_{Ly} . Free-free continuum emission is, however, optically thin at 100 GHz, so there may exist some overlap of the starburst regions, since M82 is an edge-on galaxy. We therefore evaluated the effect of overlapping based on the

structure of the superbubble and estimated that a few GMCs can overlap at Peaks D and G, since the shell structure is parallel to the line-of-sight. However, there may be none at Peaks E and F, which are close to the bubble center (i.e., the shell structure is perpendicular to the line-of-sight). There is also a possibility that starburst regions around the superbubble overlap with starburst regions in the background disk. This possibility is, however, very small, because stars are formed from molecular gas, and almost all the molecular gas toward the superbubble is dynamically associated with it (Neininger et al. 1998; Weiss et al. 1999; Wills et al. 1999; Matsushita et al. 2000). In addition, radio recombination lines, which also trace star forming regions, toward the superbubble are also dynamically associated with it (see §4.3.2). These discussions indicate that Peaks E and F are starburst regions at the inner edge of the superbubble with no overlap, and we therefore compare N_{Ly} at Peaks E and F with those at active star forming GMCs in our Galaxy and nearby galaxies.

At Peaks E and F, N_{Ly} are 5.2×10^{52} and 5.0×10^{52} photons s^{-1} for $T_{\text{e}} = 5,000$ K and 3.8×10^{52} and 3.6×10^{52} photons s^{-1} for $T_{\text{e}} = 10,000$ K, respectively (see Table 1). These N_{Ly} are an order of magnitude higher than those of active star forming regions in our Galaxy: The most massive and luminous optically visible giant H II region NGC 3603 (Goss & Radhakrishnan 1969), which is ~ 10 kpc away from the Galactic Center, has N_{Ly} of 1.1×10^{51} photons s^{-1} (Smith, Biermann, & Mezger 1978). The H II region complex G49.5 – 0.4 in one of the most luminous star forming regions W51, which is 7.6 kpc away from the Galactic Center (Smith et al. 1978), has N_{Ly} of 8.9×10^{50} photons s^{-1} (Okumura et al. 2000a). The diameters of these regions are about 50 pc and 30 pc, respectively (Okumura et al. 2000a), which are almost the same linear scale as Peaks E and F. This comparison indicates that the ongoing starburst regions in M82 are at least 30 times more active in terms of ionizing flux than the active star forming regions in our Galaxy.

Millimeter-wave (3.4 mm or 88 GHz) continuum image toward the center of the nearby spiral galaxy IC 342 show a continuum peak at a star forming GMC (cloud B in Downes et al. 1992). The peak intensity is 3.3 ± 0.6 mJy beam $^{-1}$ with the beam size of $2''.7 \times 2''.7$ (24 pc \times 24 pc at $D = 1.8$ Mpc; McCall 1989), and seems to be dominated by free-free emission. Substituting these values in Eq. 1, N_{Ly} can be calculated as $(1.7 \pm 0.3) \times 10^{51}$ photons s^{-1} for $T_{\text{e}} = 5,000$ K and $(1.2 \pm 0.2) \times 10^{51}$ photons s^{-1} for $T_{\text{e}} = 10,000$ K. H α and Pa α emission line observations toward the central $3' - 4'$ region of grand-design spiral galaxy M51 using the WFPC2 and NICMOS instruments on the Hubble Space Telescope depicted more than 1000 H II regions with their typical sizes of 10 – 100 pc (Scoville et al. 2001). The fraction of the sizes of H II regions peak around 20 – 40 pc, which is independent of their locations (including nuclear, arm, and interarm regions). The N_{Ly} of the H II regions with the sizes less than 50 pc show $\sim 7 \times 10^{50}$ photons s^{-1} . In both galaxies, star formation activities in terms of ionizing flux with the scale of 30 – 40 pc show an order of magnitude lower than

the starburst GMCs in M82.

Comparisons between starburst GMCs in M82 and star forming GMCs in our Galaxy, M51, and IC 342 suggest that the star formation in M82 is quantitatively different from those in our Galaxy, M51 and IC 342, namely, M82 has an order of magnitude higher star formation efficiency in GMC scale. Recent high angular resolution optical and near infrared observations toward nearby galaxies show many super star clusters (SSCs) with their size at most 10 pc. Our observations are limited by the beam size of 30 – 40 pc, thus we cannot compare them directly. It will be interesting to perform sub-arcsec resolution (< 20 pc) 100 GHz continuum observations toward these starburst regions in M82 to resolve SSCs and compare with those of other galaxies in the future. These observations may help to understand what causes the qualitative differences between starburst GMCs in M82 and star forming GMCs in our Galaxy and nearby galaxies.

4.2. Stellar Compositions in the Ongoing Starburst Regions

In the previous section, we estimated the production rates of Lyman continuum photons (N_{Ly}) from the ongoing starburst regions in M82. Based on this information, it is possible to estimate the stellar compositions in the starburst regions by assuming a mass function (MF).

4.2.1. Mass Function Calculations

We adopted an extended Millar-Scalo MF of $dN/dm \propto m^{-2.5}$ with lower and upper mass limits of 1 and 100 M_{\odot} (Kennicutt 1983). To estimate the total N_{Ly} from all the stars calculated from the MF, the value of N_{Ly} from stars with each stellar mass is needed. We used the stellar model of Vacca, Garmany, & Shull (1996), who calculated N_{Ly} for the O-type and early B-type stars, and their evolutionary mass model (stellar mass derived from an evolutionary track) for the luminosity class V (main sequence). The reason for using this class is the following: Since the ongoing starburst regions are located just at the inner edge of the superbubble, and these seem to be induced by the past starburst that made the superbubble (see §4.3), it is reasonable to suppose that the present starburst regions are younger than the expanding timescale of the superbubble. The age of the superbubble is about $(1 - 2) \times 10^6$ years (Weiss et al. 1999; Matsushita et al. 2000; Wills et al. 2002); hence the starburst should have occurred on less than this timescale, which is similar to or less than the lifetime of early-type stars. It is therefore appropriate to assume that all the stars

in the present starburst regions are still on the main sequence.

Since the calculations of the stellar model in Vacca et al. (1996) are done with each spectral type, we interpolated their N_{Ly} for the smaller interval of the stellar mass with fourth-order polynomial fitting. The fitting residual is 1.2%, which is much smaller than other errors (e.g., statistical noise and absolute flux error of our observations). The extrapolations for very massive stars and for late-type stars (later than late B-type stars) were done with the same function as the interpolation. Using this “interpolated/extrapolated N_{Ly} - stellar mass” relation and the MF explained above, we calculated the stellar compositions for each starburst region (Peaks A-G). The calculated stellar numbers with mass larger than $8 M_{\odot}$, which are the progenitors of supernovae, are summarized in Table 1.

We also estimated the dependence of MF slopes and stellar mass limits. If we apply a steeper MF of $dN/dm \propto m^{-3.0}$, which is close to the slope of Miller-Scalo solar neighborhood MF of -3.3 (Miller & Scalo 1979), the calculated $> 8 M_{\odot}$ stellar numbers will increase about a factor of 2. On the other hand, if we apply a shallower MF of $dN/dm \propto m^{-2.0}$, the calculated $> 8 M_{\odot}$ stellar numbers will decrease about a factor of 2. If we lower the upper mass limit to $50 M_{\odot}$, the calculated $> 8 M_{\odot}$ stellar numbers will increase about a factor of 2. Changing the lower mass limit affects to the calculations only slightly, since low mass stars emit small amounts of Lyman continuum photons. Rieke et al. (1993) computed the starburst model for M82, and concluded that the MF model of $dN/dm \propto m^{-3.0}$ with the upper mass limit of $80 M_{\odot}$ will fit their observations the best. Förster Schreiber et al. (2003) also performed starburst model calculations, and found out that their data are consistent with the MF model of $dN/dm \propto m^{-2.35}$ with the upper mass limit of $\gtrsim 50 - 100 M_{\odot}$. In either case, the difference between our and their MF models will not produce an order of magnitude difference in the calculated $> 8 M_{\odot}$ stellar numbers.

There is also a possibility that the superbubble expansion timescale is longer than the previous estimation of $(1 - 2) \times 10^6$ years. This timescale is calculated with [the size of the superbubble]/[expansion velocity], but if the acceleration of the molecular gas to the present expansion velocity is gradual (i.e., if the expansion velocity is slow when the superbubble is small), the expansion timescale should be longer than the estimation. If this is the case, some of the highest mass stars should have already been exploded by supernovae, and this effect should be considered in the MF calculations. This effect corresponds to lowering the upper mass limit of the MF calculations and, therefore, increasing the $> 8 M_{\odot}$ stellar numbers. The superbubble expansion timescale shorter than $(1 - 2) \times 10^6$ years can also be possible, due to the deceleration of the expanding velocity (Weiss et al. 1999; García-Burillo et al. 2001). In this case, the timescale is shorter than the age of the high-mass (OB type) stars, and we can assume that there are no supernova explosions in the past. Therefore, this case

does not affect any MF calculations.

4.2.2. *Estimated Supernova Energy Release from the Ongoing Starburst Regions*

It is interesting to find out whether the present starburst is more active than the past starburst that made the molecular superbubble. In order to compare the energetics of the present starburst with that of the molecular superbubble, we calculated $> 30 M_{\odot}$ stars, whose lifetime corresponds to the dynamical timescale of the superbubble of 10^6 years, at Peaks E and F. We found $\sim (12 \pm 1) \times 10^2$ stars for $T_e = 5,000$ K and $\sim (9 \pm 1) \times 10^2$ stars for $T_e = 10,000$ K, which corresponds to about 10^3 supernova explosions with a total energy release of $\sim 10^{54}$ ergs.

The efficiency of the supernova explosion energy input to the bubbles/chimneys varies. A single supernova explosion releases its energy to the surrounding ISM with an efficiency of 3 – 8%, depending on the density of the ISM (Chevalier 1974). Multiple supernova explosions, on the other hand, release their energy into the ISM more efficiently, with up to 20% of their total energy (McCray & Kafatos 1987). If we take the efficiency of 3 – 20%, bubbles/chimneys with energy of 10^{52-53} ergs will be produced at Peaks E and F in the future, which is similar to the observed bubbles in our Galaxy or nearby galaxies (e.g., Tenorio-Tagle & Bodenheimer 1988; Martin 1998). This energy is, however, a few orders of magnitude lower than that of the molecular superbubble in M82 ($\sim (0.5 - 2) \times 10^{55}$ ergs; Matsushita et al. 2000) and suggests that the present starburst regions are less active than the starburst that made the molecular superbubble.

This possibility may not be the case if the expansion timescale of the superbubble is longer than expected. The longer timescale increases the energy release from the present starburst regions owing to the increase in the number of supernovae (see §4.2.1). The energy input into the surrounding ISM, therefore, would be closer to the energy of the present superbubble.

4.3. **Induced Starburst at the Inner-Edge of the Superbubble**

4.3.1. *Structure of the Superbubble*

Molecular emission from the superbubble is strong in the southern part, but weak in the northern part. On the other hand, the images of atomic and ionized gas — H I absorption line (Wills et al. 2002), radio recombination line (H41 α ; Seaquist et al. 1996) and forbidden

line ([Ne II]; Achtermann & Lacy 1995) — show stronger intensity from the northern part than from the southern part (Fig. 5a; see also Wills et al. 1999, 2002). The shell-like structure detected in the 408 MHz continuum by Wills et al. (1997) clearly shows the complete superbubble structure. These results seem to indicate that *the superbubble is not disrupted yet*, and the southern part of the superbubble is dominated by molecular gas and the northern part by atomic and ionized gas.

The reason for this asymmetry is not clear. One possibility is that the explosions, which made the superbubble, have occurred preferentially north of the galactic disk. This initial condition suggests that the southern part is rich in molecular gas, but the northern part is not, so that the latter is more likely to be dominated by atomic and ionized gas (i.e., less molecular gas and/or less self-shielding of the molecular gas). Indeed, the large-scale (kpc-scale) H α image of M82 shows that the southern outflow is relatively confined to the minor axis of the galaxy, but the northern outflow has a wider opening angle. This difference suggests that the starburst is located slightly north of the galactic disk, and the material distribution asymmetry causes the different collimations in the northern and southern outflows (Shopbell & Bland-Hawthorn 1998). Such asymmetry in the structure of bubbles can also be seen in other galaxies (e.g., our Galaxy, Normandeau, Taylor, & Dewdney 1996; M101, Kamphuis, Sancisi, & van der Hulst 1991), although their low-density regions are thought to be already disrupted.

4.3.2. Kinematics of Ionized Gas

We compared the position-velocity (PV) diagram of molecular gas with that of a radio recombination line (H41 α ; Seaquist et al. 1996) and found that *the deviation from the rigid rotation of the recombination line is larger than that of the molecular gas* (Fig. 5b). Similar deviation difference is also seen in the comparison between the molecular gas and the [Ne II] line (Wills et al. 1999). Since the deviation is evidence of the superbubble expansion (Neininger et al. 1998; Weiss et al. 1999; Wills et al. 1999; Matsushita et al. 2000; Wills et al. 2002), the ionized gas is kinematically related to the superbubble, but moves faster than the neutral gas.

4.3.3. Distributions and Kinematics of Masers

We compiled all the observed OH and H₂O masers toward M82 (Weliachew, Fomalont, & Greisen 1984; Baudry & Brouillet 1996; Seaquist, Frayer, & Frail 1997) and found that *the*

masers are obviously concentrated at the 100 GHz continuum emitting regions, namely, the intense starburst regions (Fig. 2). In addition, we overplotted the masers on the PV diagram of molecular gas and found that the OH and H₂O masers are strongly concentrated at the superbubble with good velocity coincidences (Fig. 5b). Pumping mechanisms for OH masers are collisions (\approx shocks) and/or IR/UV radiation (\approx radiation from H II regions), and those for H₂O masers are basically shocks (Elitzur 1992).¹ Indeed, observations of our Galaxy indicate that these masers can be seen around H II regions (Gaume & Mutel 1987; Elitzur 1992) and at the shock fronts of supernova remnants (Arikawa et al. 1999). Furthermore, masers in M82 are not so luminous as megamasers around AGNs, but much more similar to the Galactic sources (Baudry & Brouillet 1996; Seaquist et al. 1997). In addition, recent interferometric SiO line observations toward the superbubble suggest that the SiO line may trace shocked regions, and the shocked regions may locate the inner wall of the superbubble (García-Burillo et al. 2001), consistent with our result.

4.3.4. Distribution of Diffuse Hard X-ray Emission

Both inside and outside the superbubble, various X-ray sources can be seen from soft/medium ($\sim 0.1 - 2$ keV) to hard components ($\sim 3 - 10$ keV). The soft and medium components show extended structures, which are believed to originate from hot thermal plasma (Tsuru et al. 1997; Strickland et al. 1997; Griffiths et al. 2000). The soft component corresponds well with the large-scale ionized gas outflows (Watson et al. 1984; Kronberg et al. 1985; Strickland et al. 1997; Shopbell & Bland-Hawthorn 1998). However, the medium component is much more concentrated (Tsuru et al. 1997), and its peak position is located at the center of the superbubble (Matsushita et al. 2000; Matsumoto & Tsuru 1999). Most of the hard component, on the other hand, comes from point sources (Tsuru et al. 1997), which are thought to be neutron stars, stellar-mass black holes, and an intermediate-mass black hole (Matsumoto & Tsuru 1999; Ptak & Griffiths 1999; Matsushita et al. 2000; Matsumoto et al. 2001; Kaaret et al. 2001). Some fraction of the hard component, however, comes from a diffuse source with an extent of $7''.2 \times 5''.4$ (Griffiths et al. 2000). Figure 6 shows the diffuse hard X-ray image (thick contour map; Griffiths et al. 2000) overlaid on

¹Strictly speaking, H₂O maser sources need to have (1) high H₂ number density of $\sim 10^9$ cm⁻³, (2) high temperature of ~ 400 K, and (3) pumping sources. In our Galaxy, the maser-emitting sources are usually shocked molecular gas, but in the center of galaxies, dense molecular gas disks/tori around active galactic nuclei (AGNs) are also possible, such as H₂O megamasers toward the AGN of NGC 4258 (Miyoshi et al. 1995). As mentioned below, since the luminosity of H₂O masers in M82 is similar to the Galactic sources, we think H₂O masers in M82 are coming from shocked molecular gas.

the the $^{12}\text{CO}(1 - 0)$ superbubble image (thin contour with greyscale map; Matsushita et al. 2000). The diffuse hard X-ray emission is extended toward the center of the galaxy, but the peak is located inside of the molecular superbubble. Since the diffuse hard X-ray data do not have any line-of-sight information, we do not know where is the actual location(s) of the emitting source(s), but clearly there is some source toward the inner part of the superbubble. This position correspondence suggests that some of the diffuse hard X-ray component locates inside the superbubble.

This component could be due to hot thermal plasma (Griffiths et al. 2000), which is also supported by 408 MHz observations (free-free absorption has been detected at the superbubble; Wills et al. 1997), but the possibility of inverse Compton scattering cannot be ruled out (Griffiths et al. 2000). Assuming that the diffuse hard X-ray component is caused by hot thermal plasma, we can calculate the velocity of the plasma. The sound speed, i.e., the velocity, of protons, C_p , in the plasma can be expressed as $C_p \sim \sqrt{kT/m_p}$, where k is the Boltzmann constant, T is temperature (K), and m_p is the proton mass. Since the plasma temperature, kT , is estimated as 2.4 – 4.1 keV (Griffiths et al. 2000), the velocity can be calculated as $C_p \sim (5 - 6) \times 10^2 \text{ km s}^{-1}$. This number is 5 – 12 times faster than the expansion velocity of the superbubble, hence the superbubble should be closed and the plasma should be overpressurized, if the plasma is in the superbubble. Indeed, the superbubble seems to be closed (§4.3.1), and Griffiths et al. (2000) suggest that the plasma seems to be overpressurized. In addition, the expansion velocity of the ionized gas² in the superbubble is faster than that of the molecular gas, and masers are concentrated at the superbubble (§4.3). These support the idea that the some of the diffuse hard X-ray component is located inside the superbubble.

As mentioned above, the possibility that the diffuse hard X-ray component might originate from inverse Compton scattering cannot be ruled out (Griffiths et al. 2000). If true, it indicates that nonthermal high-energy electrons are strongly concentrated inside the superbubble, because the diffuse hard X-ray emission peaks at there. The trapping mechanism of the nonthermal high-energy electrons is unclear, but the magnetic field in and around the superbubble may be playing an important role.

²In this paper, we used “ionized gas” as 10^4 K gas that can be seen with recombination lines, and “hot plasma” as 10^7 K gas that can be seen with thermal X-ray emission, to distinct these two kind of gas.

4.3.5. Induced Starburst

In summary, the expanding superbubble seems to be still closed, the overpressurized hot plasma may be filling inside of the superbubble, ionized gas is spatially and kinematically correlated with the expansion of superbubble but moves faster, the masers are also spatially and kinematically located at the inner edge of the superbubble, and the free-free emission is located at the inner edge of the superbubble. The configuration of plasma, ionized gas, and superbubble is very similar to that of the expanding supernova remnants in our Galaxy (e.g., White & Long 1991); recombination lines that traces ionized gas emit from shock-heated gas and the gas evaporate from the surrounding material that forms shell structures. The faster velocity than the surrounding molecular superbubble and the existence of the masers support this idea. These structural and kinematical features therefore suggest that *the hot plasma expanded the superbubble, created the shocked regions at the inner-edge of the superbubble, and induced the active starbursts at there.*

Sequential star formation in molecular clouds induced by expanding ionized gas (\approx shocks) has been suggested theoretically (e.g., McCray & Kafatos 1987; Elmegreen & Lada 1977). In our Galaxy, this sequential star formation has also been suggested observationally (e.g., Sugitani et al. 1989; Sugitani, Tamura, & Ogura 1995; Yamaguchi et al. 1999). In addition, these observational papers suggest that the induced star forming regions tend to make more massive stars than isolated quiescent dark clouds. We therefore conclude that the present starburst (massive star forming) regions in M82 are induced in ways similar to those of the sequential star formation regions in our Galaxy.

At the center of the superbubble, on the other hand, there is almost no molecular gas emission, neither diffuse (^{12}CO) nor dense (HCN), from both spatial and dynamical points of view (Figs. 2, 5b; see also Matsushita et al. 2000). Furthermore, the 100 GHz continuum emission is also weak at this region compared to the inner edge of the superbubble (see Fig. 3). Since stars are believed to be made from molecular clouds, especially from dense parts (e.g., Lada 1992; Solomon, Downes, & Radford 1992; Kohno, Kawabe, & Vila-Vilaró 1999), and free-free (100 GHz continuum) emission is produced by massive stars, these suggest that the starburst at the center of the superbubble begins to cease, and the number of massive stars is decreasing by supernova explosions.

From these results and discussions, we propose an evolution of starburst around the superbubble in M82. First, the energetic explosions occurred as a consequence of the localized starburst at the center of the superbubble (Matsushita et al. 2000). The resultant shock waves ionized the surrounding ISM, produced the hot thermal plasma and ionized gas, and swept them outward. The neutral ISM (e.g., molecular gas), had also been swept outward and produced the expanding molecular superbubble. Most of the molecular gas at the central

starburst region was blown away and/or ionized by the energetic explosions and/or by the strong UV radiation from massive stars, so that the starburst begins to cease. The expansion of the superbubble inside the galactic disk, which is rich in ISM, had compressed the ISM and caused a concentration around the superbubble. This concentration appears as double peaks by the edge-brightening effect (Wills et al. 1999), and these double peaks correspond to the well known “central peak” and the inner side of the “SW lobe,” which can be seen in molecular gas images (e.g., Carlstrom & Kromberg 1991; Shen & Lo 1995). The inner edge of this concentration is the shock front of the superbubble expansion, which caused the shocked regions and induced star forming regions in the molecular gas, and produced the masers and free-free continuum emissions at these regions. These induced star forming regions correspond to the present starburst regions in M82. This result is the first clear evidence of self-induced starburst in an external galaxy.

The size-scale of this self-induced starburst is rather small, about 200 pc, and located off from the nucleus (see Fig. 2). This localized and offset self-induced starburst may be the cause of inconsistent conclusions of inward/outward starburst propagations (see §1). The detailed studies at various wavelengths with comparing the positions of superbubbles (e.g., Wills et al. 2002) will give us the detailed starburst propagation and evolution mechanisms.

4.4. Starburst Timescale

Recent observations and model calculations suggest that the central region of M82 has experienced at least two starbursts within $\sim 10^7$ years. Optical emission line study suggests that the large-scale outflows originate from at least two (Shopbell & Bland-Hawthorn 1998), maybe several (Martin 1998) different burst regions. Model calculations based on infrared spectroscopic observations required two starbursts within $\sim 10^7$ years. The first starburst can be explained by the large-scale outflows and red supergiants, and the second one by the UV flux (Rieke et al. 1993; Förster Schreiber et al. 2003). The molecular and dust outflows, which can be seen in both interferometric (Matsushita et al. 2000; Walter et al. 2002) and single-dish observations (Nakai et al. 1987; Kuno & Matsuo 1997; Alton et al. 1999; Taylor et al. 2001), extend not only from the superbubble region, but also everywhere from the molecular disk.

Our observations, on the other hand, show the past starburst, which has made the superbubble (expansion timescale of $\sim (1 - 2) \times 10^6$ years; §4.2.1), and the present induced starburst, which is believed to be younger than the expanding timescale of the superbubble (§4.2). In addition, the superbubble still has closed structure (§4.3.1 and 4.3.4). Furthermore, numerical simulations indicate that large-scale outflows are created by energetic starbursts

that can produce superbubbles (e.g., Tomisaka & Ikeuchi 1988).

These observations and simulations indicate that the energetic starbursts in M82, which produced the large-scale outflows, occurred at least twice in this $\sim 10^7$ years, and the recent starbursts (the starburst that made the superbubble and the present starburst) occurred on an order-of-magnitude shorter timescale. These indications suggest that several starbursts had occurred in this $\sim 10^7$ years. It is not clear whether starbursts occurred intermittently or continuously within 10^6 years or shorter timescale. However, if you average over long timescale, say order of 10^{7-8} years, starburst in M82 seems occurring continuously, with the self-induced mechanism. This self-induced starburst would continue till most of the molecular gas is consumed by the star formation, blown away from the disk region of the galaxy, and/or is dissociated by strong UV radiation, and this timescale may correspond to the timescale of the whole starburst phenomena of 10^{7-8} years (e.g., Rieke 1988; Heckman 1998).

These self-induced/self-regulating mechanisms would be very important for other starburst galaxies. Recent optical spectroscopic and X-ray observations show that most of starburst galaxies have large-scale outflows (e.g., Lehnert & Heckman 1996; Martin 1998; Dahlem et al. 1998). Mid-infrared observations of starburst galaxies indicate that the timescale of most starbursts are $10^6 - 10^7$ years (e.g., Thornley et al. 2000; Vanzi et al. 1998). These results are consistent with those of M82, and strongly suggest that most of the starbursts would have experienced similar starburst evolution as M82.

5. CONCLUSIONS

Our new high spatial resolution 100 GHz continuum (i.e., free-free emission) image in the central region of M82 clearly shows that present starburst regions are strongly concentrated at the inner edge of the expanding molecular superbubble. The Lyman continuum photon numbers from the starburst regions (i.e., the strength of the starburst) are an order of magnitude larger than those in the active high-mass star forming regions in our Galaxy (NGC 3603 and W51) and nearby galaxies (IC 342 and M51).

The internal structure of the present superbubble, from the center, shows a red supergiant star cluster (“ $2.2 \mu\text{m}$ secondary peak”), overpressurized hot thermal plasma or high energy electrons (diffuse hard X-ray emission), high velocity ionized gas (H41 α and [Ne II]), shocked molecular gas (masers and SiO emission) and the present starburst regions (free-free emission), and the expanding molecular superbubble located furthermost outside. This structure and the physical properties of these objects/mediums suggest that the present star-

burst has been induced by the past starburst that made the superbubble, namely, self-induced starburst. The existence of kpc-scale outflows, a few hundred parsec-scale superbubble, and induced starburst inside the superbubble suggest that the starbursts in M82 have occurred several times in this 10^6 – 10^7 years. Since the appearance of the starburst (e.g., outflows) in M82 is typical in other starburst galaxies, this starburst mechanism will be very important for the studies of other starburst regions/galaxies and galaxy formation.

We would like to thank P. T. P. Ho, N. Fukuda, S. Ikeuchi, M. Saito, K. Sugitani, and anonymous referee for helpful discussions and comments. We also thank A. F. Omundsen for carefully reading our manuscript. Thanks are also due to Y. Ohyama for providing the Subaru H α image for us. We are grateful to the NRO staff for the operation and improvement of NMA.

REFERENCES

Achtermann, J. M., & Lacy, J. H. 1995, *ApJ*, 439, 163

Alton, P. B., Davies, J. J., & Bianchi, S. 1999, *A&A*, 343, 51

Arikawa, Y., Tatematsu, K., Sekimoto, Y., & Takahashi, T. 1999, *PASJ*, 51, L7

Baudry, A., & Brouillet, N. 1996, *A&A*, 316, 188

Bregman, J. N., Schulman, E., & Tomisaka, K. 1995, *ApJ*, 439, 155

Brouillet, N., & Schilke, P. 1993, *A&A*, 277, 381

Carlstrom, J. E., & Kromberg, P. P. 1991, *ApJ*, 366, 422

Chevalier, R. A. 1974, *ApJ*, 188, 501

Condon, J. J. 1992, *ARA&A*, 30, 575

Cottrell, G. A. 1977, *MNRAS*, 178, 577

de Grijs, R., O'Connell, R. W., & Gallagher, J. S., III 2001, *AJ*, 121, 768

Dahlem, M., Weaver, K. A., & Heckman, T. M. 1998, *ApJS*, 118, 401

Dietz, R. D., Smith, J., Hackwell, J. A., Gehrz, R. D., & Grasdalen, G. L. 1986, *AJ*, 91, 758

Downes, D., Radford, S. J. E., Guilloteau, S., Guélin, M., Greve, A., & Morris, D. 1992, *A&A*, 262, 424

Draine, B. T. 1989, in *Infrared Spectroscopy in Astronomy*, ed. B. H. Kaldeich (Noordwijk: ESTEC), 93

Elitzur, M. 1992, *Astronomical Masers* (Dordrecht: Kluwer)

Elmegreen, B. G., & Lada, C. J. 1977, *ApJ*, 214, 725

Förster Schreiber, N. M., Genzel, R., Lutz, D., Kunze, D., & Sternberg, A. 2001, *ApJ*, 552, 544

Förster Schreiber, N. M., Genzel, R., Lutz, D., & Sternberg, A. 2003, *ApJ*, 599, 193

Gallagher, J. S., III, & Smith, L. J. 1999, *MNRAS*, 304, 540

García-Burillo, S., Martín-Pintado, J., Fuente, A., & Neri, R. 2001, *ApJ*, 563, L27

Gaume, R. A., & Mutel, R. L. 1987, *ApJS*, 65, 193

Goss, W. M., & Radhakrishnan, V. 1969, *Astrophys. Lett.*, 4, 199

Griffiths, R. E., Ptak, A., Feigelson, E. D., Garmire, G., Townsley, L., Brandt, W. N., Sambruna, R., & Bregman, J. N. 2000, *Science*, 290, 1325

Heckman, T. M. 1998, in *ASP Conf. Ser.* 148, *Origins*, ed. C. E. Woodward, J. M. Shull, & H. A. Thronson (San Francisco: ASP), 127

Joy, M., Lester, D. F., & Harvey, P. M. 1987, *ApJ*, 319, 314

Jura, M., Hobbs, R. W., & Maran, S. P. 1978, *AJ*, 83, 153

Kaaret, P., Prestwich, A. H., Zezas, A., Murray, S. S., Kim, D.-W., Kilgard, R. E., Schlegel, E. M., & Ward, M. J. 2001, *MNRAS*, 321, L29

Kamphuis, J., Sancisi, R., & van der Hulst, T. 1991, *A&A*, 244, L29

Kennicutt, R. C. 1983, *ApJ*, 272, 54

Kohno, K., Kawabe, R., & Vila-Vilaró, B. 1999, *ApJ*, 511, 157

Kuno, N., & Matsuo, H. 1997, *PASJ*, 49, 265

Kronberg, P. P., Biermann, P., & Schwab, F. R. 1985, *ApJ*, 291, 693

Lada, E. A. 1992, *ApJ*, 393, L25

Lehnert, M. D., & Heckman, T. M. 1996, *ApJ*, 462, 651

Lester D. F., Carr, J. S., Joy, M., & Gaffney, N. 1990, *ApJ*, 352, 544

Lynds, C. R., & Sandage, A. R. 1963, *ApJ*, 137, 1005

Martin, C. L. 1998, *ApJ*, 506, 222

Matsumoto, H., & Tsuru, T. G. 1999, *PASJ*, 51, 321

Matsumoto, H., Tsuru, T. G., Koyama, K., Awaki, H., Canizares, C. R., Kawai, N., Matsushita, S., & Kawabe, R. 2001, *ApJ*, 547, L25

Matsuo, H., Kuno, N., Vila-Vilaró, B., Kashihara, H., & Kawabata, T. 1998, in *Central Regions of the Galaxy and Galaxies, IAU Symp.* 184, ed. Y. Sofue (Kluwer: Dordrecht), 143

Matsushita, S., Kawabe, R., Matsumoto, H., Tsuru, T. G., Kohno, K., Morita, K.-I., Okumura, S. K., & Vila-Vilaró, B. 2000, *ApJ*, 545, L107

McCall, M. L. 1989, *AJ*, 97, 1341

McCrory, R., & Kafatos, M. 1987, *ApJ*, 317, 190

McLeod, K. K., Rieke, G. H., Rieke, M. J., & Kelly, D. M. 1993, *ApJ*, 412, 111

Miller, G. E., & Scalo, J. M. 1979, *ApJS*, 41, 513

Miyoshi, M., Moran, J., Herrnstein, J., Greenhill, L., Nakai, N., Diamond, P., & Inoue, M. 1995, *Nature*, 373, 127

Nakai, N., Hayashi, M., Handa, T., Sofue, Y., & Hasegawa, T. 1987, *PASJ*, 39, 685

Neininger, N., Guélin, M., Klein, U., García-Burillo, S., & Wielebinski, R. 1998, *A&A*, 339, 737

Normandeau, M., Taylor, A.R., & Dewdney, P. E. 1996, *Nature*, 380, 687

O'Connell, R. W., & Mangano, J. J. 1978, *ApJ*, 221, 62

Ohyama, Y., et al. 2002, *PASJ*, 54, 891

Okumura, S., Mori, A., Nishihara, E., Watanabe, E., & Yamashita, T. 2000a, *ApJ*, 543, 799

Okumura, S. K., et al. 2000b, *PASJ*, 52, 393

Ptak, A., & Griffiths, R. E. 1999, *ApJ*, 517, L85

Puxley, P. J., Brand, P. W. J. L., Moore, T. J. T., Mountain, C. M., Nakai, N., & Yamashita, T. 1989, *ApJ*, 345, 163

Rieke, G. H. 1988, in *Galactic and Extragalactic Star Formation*, ed. R. E. Pudritz, & M. Fich, (Dordrecht: Kluwer), 561

Rieke, G. H., & Lebofsky, M. J. 1978, *ApJ*, 220, L37

Rieke, G. H., & Lebofsky, M. J. 1979, *ARA&A*, 17, 477

Rieke, G. H., Lebofsky, M. J., Thompson, R. I., Low, F. J., & Tokunaga, A. T. 1980, *ApJ*, 238, 24

Rieke, G. H., Loken, K., Rieke, M. J., & Tamblyn, P. 1993, *ApJ*, 412, 99

Rubin, R. H. 1968, *ApJ*, 154, 391

Sakai, S., & Madore, B. F. 1999, *ApJ*, 526, 599

Satyapal, S., et al. 1995, *ApJ*, 448, 611

Satyapal, S., Watson, D. M., Pipher, J. L., Forrest, W. J., Greenhouse, M. A., Smith, H. A., Fischer, J., & Woodward, C. E. 1997, *ApJ*, 483, 148

Scoville, N. Z., Polletta, M., Ewald, S., Stolovy, S. R., Thompson, R., & Rieke, M. 2001, *AJ*, 122, 3017

Seaquist, E. R., Kerton, C. R., & Bell, M. B. 1994, *ApJ*, 429, 612

Seaquist, E. R., Carlstrom, J. E., Bryant, P. M., & Bell, M. B. 1996, *ApJ*, 465, 691

Seaquist, E. R., Frayer, D. T., & Frail, D. A. 1997, *ApJ*, 487, L131

Shen, J., & Lo, K. Y. 1995, *ApJ*, 445, L99

Shopbell, P. L., & Bland-Hawthorn, J. 1998, *ApJ*, 493, 129

Smith, L. F., Biermann, P., & Mezger, P. G. 1978, *A&A*, 66, 65

Smith, L. J., & Gallagher, J. S., III 2001, *MNRAS*, 326, 1027

Solomon, P. M., Downes, D., & Radford, S. J. E. 1992, *ApJ*, 387, L55

Strickland, D. K., Ponman, T. J., & Stevens, I. R. 1997, *A&A*, 320, 378

Sugitani, K., Fukui, Y., Mizuno, A., & Ohashi, N. 1989, *ApJ*, 342, L87

Sugitani, K., Tamura, M., & Ogura, K. 1995, *ApJ*, 455, L39

Sunada, K., Kawabe, R., & Inatani, J. 1994, *Int. J. Infrared Millimeter Waves*, 14, 1251

Taylor, C. L., Walter, F., & Yun, M. S. 2001, *ApJ*, 562, L43

Telesco, C. M. 1993, in *Infrared Astronomy*, ed. A. Mampaso, M. Prieto, & F. Sánchez (Cambridge: Cambridge University Press), 173

Telesco, C. M., Campins, H., Joy, M., Dietz, K., & Decher, R. 1991, *ApJ*, 369, 135

Tenorio-Tagle, G., & Bodenheimer, P. 1988, *ARA&A*, 26, 145

Thornley, M. D., Schreiber, N. M. F., Lutz, D., Genzel, R., Spoon, H. W. W., Kunze, D., & Sternberg, A. 2000, *ApJ*, 539, 641

Tomisaka, K., & Ikeuchi, S. 1988, *ApJ*, 330, 695

Tsuru, T. G., Awaki, H., Koyama, K., & Ptak, A. 1997, *PASJ*, 49, 619

Tsutsumi, T., Morita, K.-I., & Umeyama, S. 1997, in *ASP Conf. Ser.* 125, *Astronomical Data Analysis Software and Systems VI*, ed. G. Hunt & H. E. Payne (San Francisco: ASP), 50

Vacca, W. D., Garmann, C. D., & Shull, J. M. 1996, *ApJ*, 460, 914

Vanzi, L., Alonso-Herrero, A., & Rieke, G. H. 1998, *ApJ*, 504, 93

Walter, F., Weiss, A., & Scoville, N. 2002, *ApJ*, 580, L21

Watson, M. G., Stanger, V., & Griffiths, R. E. 1984, *ApJ*, 286, 144

Weiss, A., Walter, F., Neininger, N., & Klein, U. 1999, *A&A*, 345, L23

Weliachew, L., Fomalont, E. B., & Greisen, E. W. 1984, *A&A*, 137, 335

White, R. L., & Long, K. S. 1991, *ApJ*, 373, 543

Wills, K. A., Pedlar, A., & Muxlow, T. W. B. 2002, *MNRAS*, 331, 313

Wills, K. A., Pedlar, A., Muxlow, T. W. B., & Wilkinson, P. N. 1997, *MNRAS*, 291, 517

Wills, K. A., Redman, M. P., Muxlow, T. W. B., & Pedlar, A. 1999, *MNRAS*, 309, 395

Yamaguchi, R., Saito, H., Mizuno, N., Mine, Y., Mizuno, A., Ogawa, H., & Fukui, Y. 1999, *PASJ*, 51, 791

Yun, M. S., Ho, P. T. P., & Lo, K. Y. 1994, *Nature*, 372, 530

Table 1. Observed and Calculated Properties of the Ongoing Starburst Regions.

Peak ^a	R.A. 09 ^h 51 ^m (B1950)	Dec. 69 ^o (B1950)	F_T ^b [mJy beam ⁻¹]	N_{Ly} ^c [photons s ⁻¹]		$N_{>8M_\odot}$ ^d	
				$(T_e = 5,000 \text{ K})$	$(T_e = 10,000 \text{ K})$	$(T_e = 5,000 \text{ K})$	$(T_e = 10,000 \text{ K})$
A	45 ⁸ .7	55'04"1	13.2	3.2×10^{52}	2.4×10^{52}	9.2×10^3	6.7×10^3
B	44 ⁸ .4	55'01"8	12.3	3.0×10^{52}	2.2×10^{52}	8.6×10^3	6.3×10^3
C	43 ⁸ .1	55'01"3	12.6	3.1×10^{52}	2.3×10^{52}	8.8×10^3	6.5×10^3
D	42 ⁸ .6	54'58"1	23.1	5.7×10^{52}	4.2×10^{52}	16.1×10^3	11.8×10^3
E	42 ⁸ .3	54'58"6	21.2	5.2×10^{52}	3.8×10^{52}	14.7×10^3	10.8×10^3
F	41 ⁸ .6	54'58"3	20.2	5.0×10^{52}	3.6×10^{52}	14.0×10^3	10.3×10^3
G	41 ⁸ .2	54'56"6	15.3	3.8×10^{52}	2.8×10^{52}	10.7×10^3	7.8×10^3

^aPeak positions are indicated in Fig. 1.

^b100 GHz continuum flux at the peak positions. The beam size is 2^{''}3 × 1^{''}9 (43 pc × 36 pc at D = 3.9 pc; Sakai & Madore 1999). 1 σ uncertainty is 2.0 mJy beam⁻¹.

^cProduction rates of Lyman continuum photons calculated with F_T averaged over the beam size. 1 σ uncertainties are 0.5×10^{52} photons s⁻¹ for $T_e = 5,000 \text{ K}$, and 0.4×10^{52} photons s⁻¹ for $T_e = 10,000 \text{ K}$. See text for details.

^dNumber of stars with their masses larger than $8 M_\odot$, assuming a mass function. 1 σ uncertainties are 1.4×10^3 for $T_e = 5,000 \text{ K}$, and 1.0×10^3 for $T_e = 10,000 \text{ K}$. See text for details.

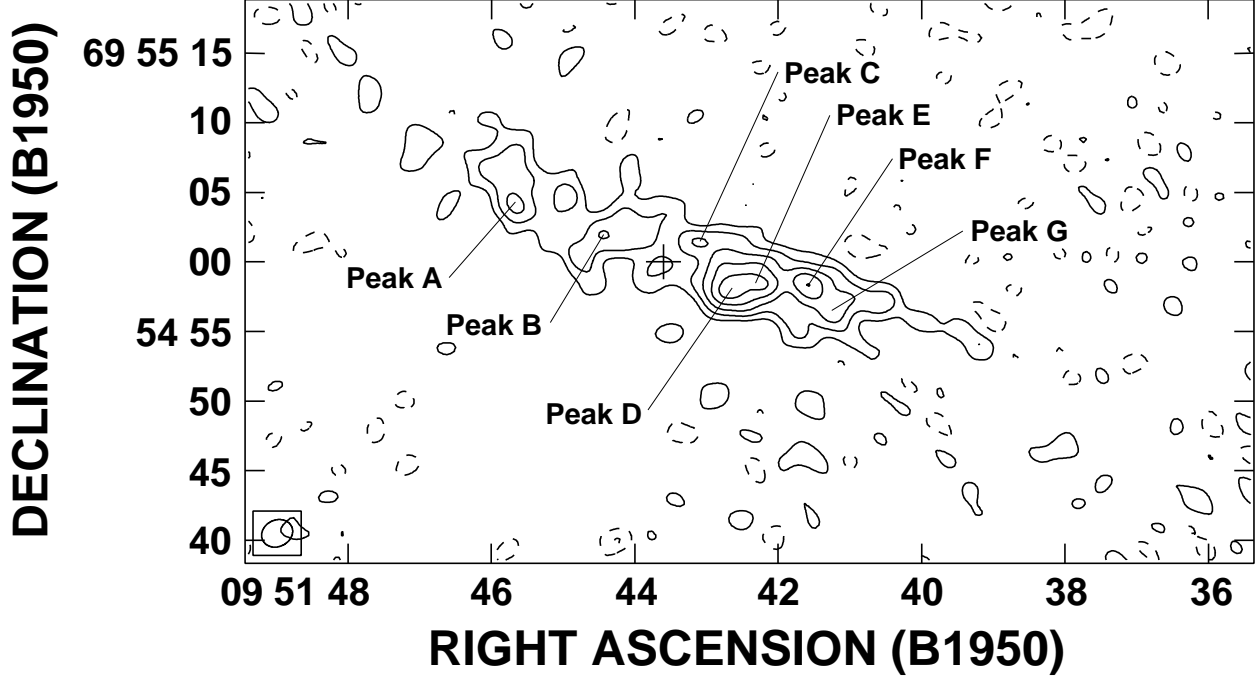


Fig. 1.— Uniform uv weighting 100 GHz continuum image of the central region of M82. The contour levels of the map are $-4, -2, 2, 4, 6, 8$, and 10σ , where $1\sigma = 2.0$ mJy beam $^{-1}$. The synthesized beam ($2.^{\prime\prime}3 \times 1.^{\prime\prime}9$ or 43 pc \times 36 pc) is shown at the bottom-left corner. The plus mark indicates the position of the galactic nucleus determined from the peak of the strongest 2.2 μ m source of $\alpha(\text{B1950})=9^{\text{h}}51^{\text{m}}43^{\text{s}}.6$ and $\delta(\text{B1950})=69^{\circ}55'00''$ (Lester et al. 1990). Peaks A-G are labeled in the image.

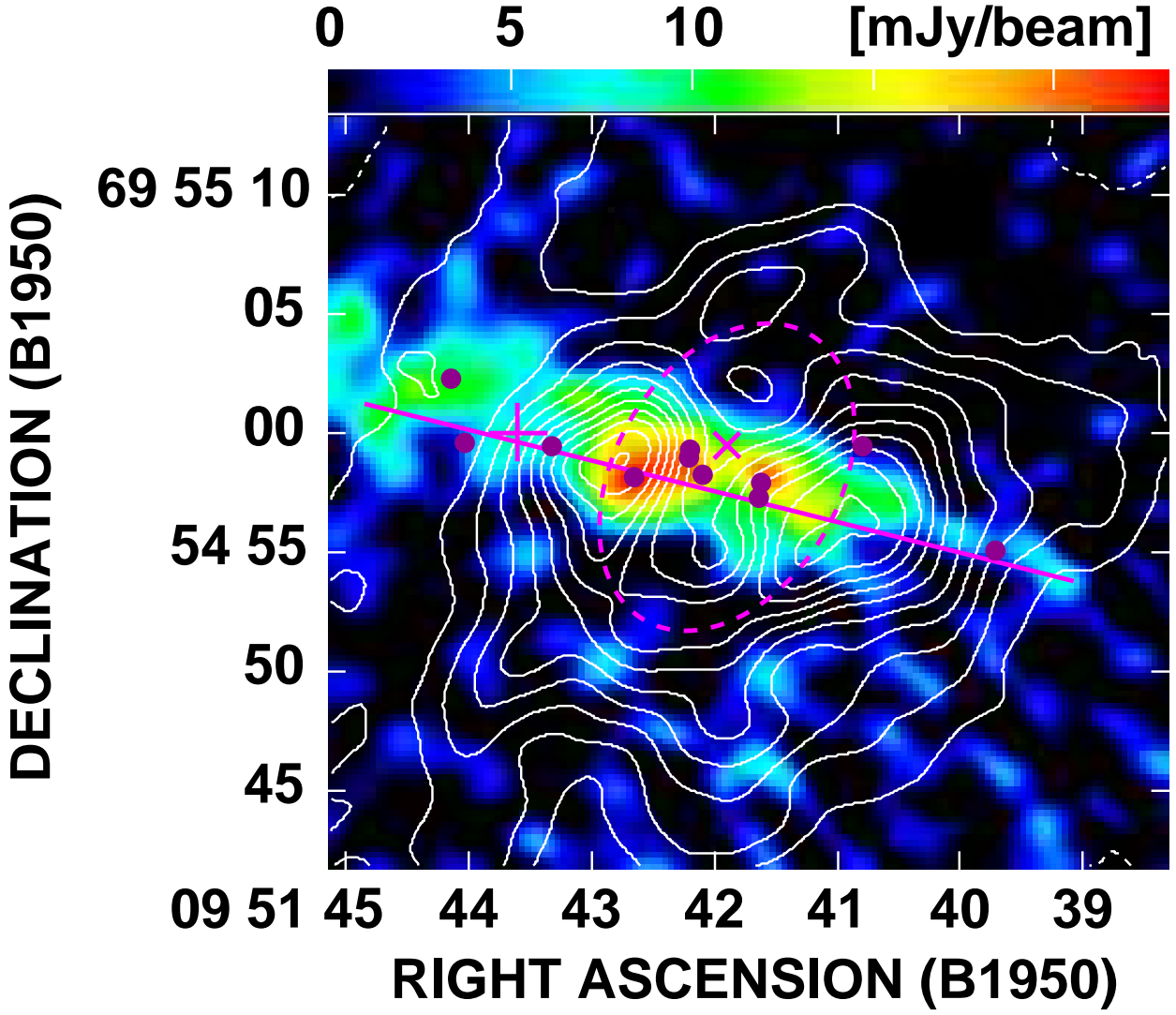


Fig. 2.— $^{12}\text{CO}(1 - 0)$ image (contours; Matsushita et al. 2000) overlaid on 100 GHz continuum image (colorscale). Values for the colorscale are indicated on the top of the figure. The dashed line (magenta) illustrates the outline of the molecular superbubble. The solid line (magenta) indicates the sliced region for the intensity plots of the superbubble shown in Fig. 3. The plus mark (magenta) is the same as Fig. 1, and the cross mark (magenta) indicates the central position of the “ $2.2 \mu\text{m}$ secondary peak” (Dietz et al. 1986). The filled purple circles indicate the positions of the OH and H_2O masers (Weliachew et al. 1984; Baudry & Brouillet 1996; Seaquist et al. 1997).

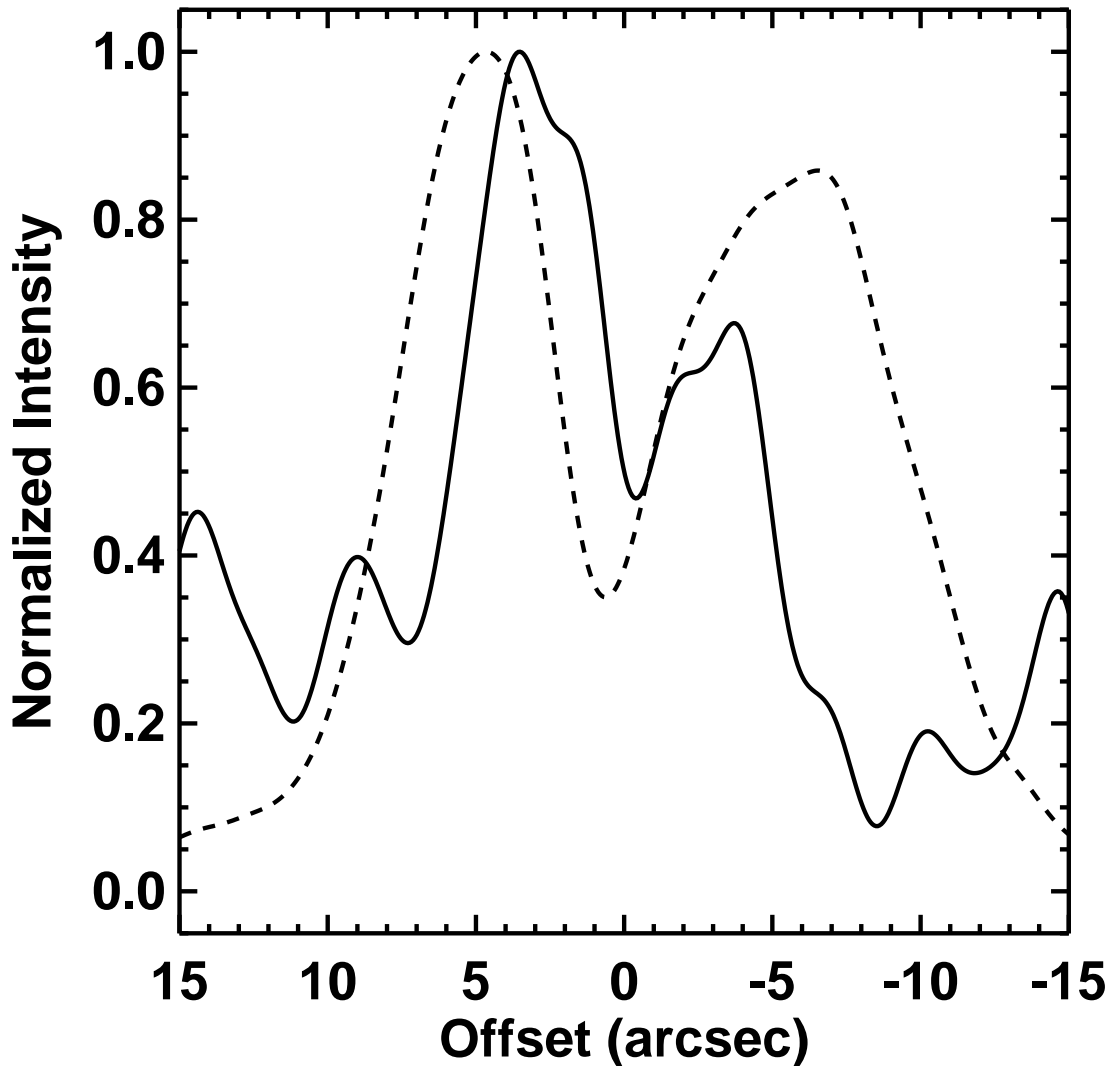


Fig. 3.— 100 GHz continuum (solid line) and $^{12}\text{CO}(1 - 0)$ (dashed line) intensity plots of the superbubble sliced along the major axis (P.A. = 76°), namely along the disk, of the galaxy. The vertical axis is normalized intensity, and the horizontal axis is offset from the center of the molecular superbubble, which is $\alpha(\text{B1950})=9^{\text{h}}51^{\text{m}}41\text{s.9}$ and $\delta(\text{B1950})=69^\circ54'57\text{.6}$.

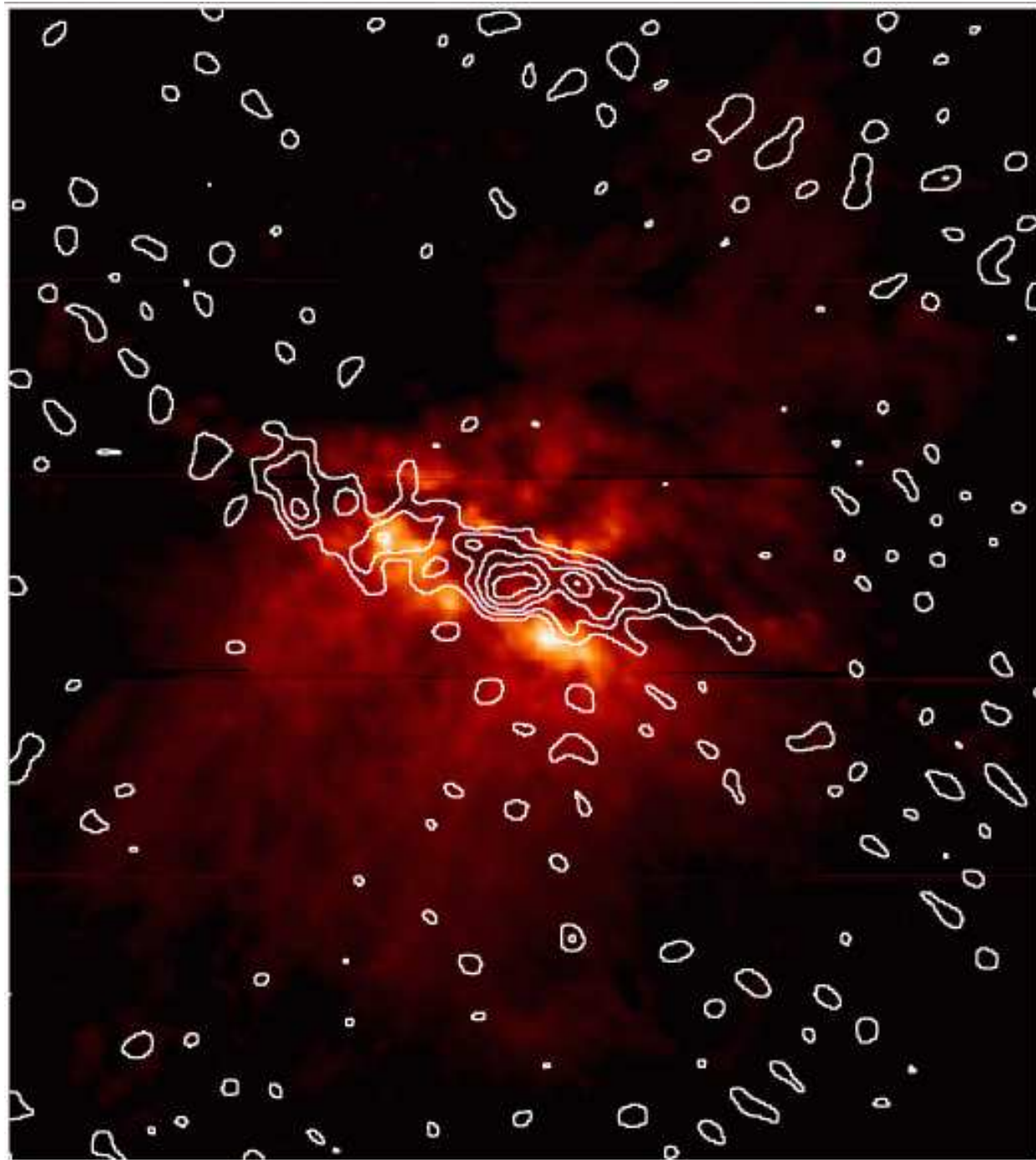


Fig. 4.— H α narrow band image taken by the Subaru 8 m telescope (colorscale map; Ohyama et al. 2002) overlaid on the 100 GHz continuum image (contour map). The contour scale is the same as in Fig. 1.

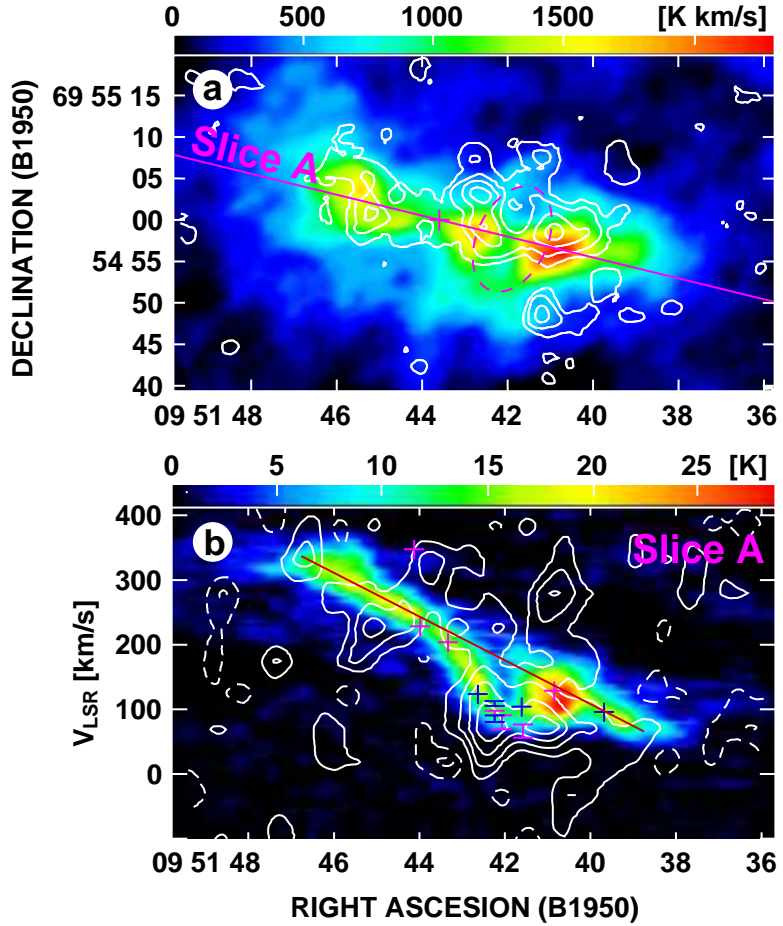


Fig. 5.— (a) H41 α integrated intensity image (contours; Seaquist et al. 1996) overlaid on the $^{12}\text{CO}(1 - 0)$ integrated intensity image (colorscale; Matsushita et al. 2000). Values for the colorscale are indicated on the top of the figure. Dashed line (magenta) shows the brief structure of the molecular superbubble. Solid line (magenta) indicates the sliced region for a position-velocity (PV) diagram indicated below. The plus mark (magenta) is the same as Fig. 1. (b) PV diagram at the slice A. H41 α image (contours; Seaquist et al. 1996) overlaid on the $^{12}\text{CO}(1 - 0)$ image (colorscale; Matsushita et al. 2000). Values for the colorscale are indicated on the top of the figure. Solid line (red) indicates the rigid rotation velocity. Plus marks indicate OH (magenta; Welichew et al. 1984; Seaquist et al. 1997) and H₂O (blue; Baudry & Brouillet 1996) masers with small velocity range. Bar marks indicate OH (magenta) and H₂O (blue) masers with velocity ranges indicated by the bars. H41 α emission shows much larger deviation from the rigid rotation velocity than that of the molecular gas at the region of the superbubble (around $\alpha(\text{B1950})=9^{\text{h}}51^{\text{m}}42^{\text{s}}$). At this region, OH and H₂O masers are dynamically concentrated.

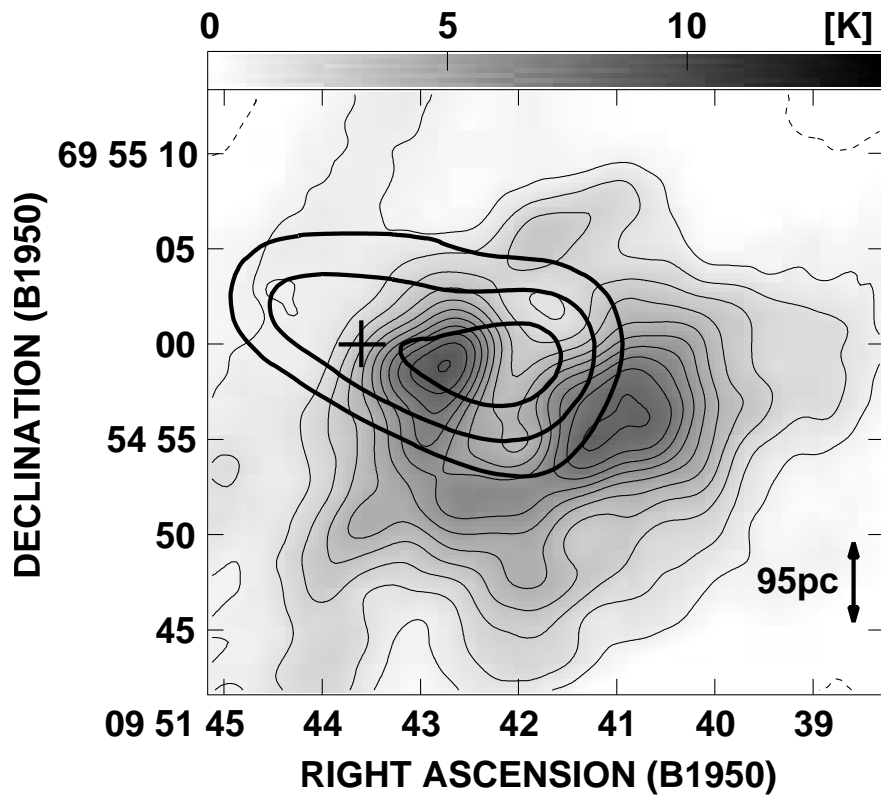


Fig. 6.— Diffuse hard X-ray image (thick contour map; Griffiths et al. 2000) overlaid on the $^{12}\text{CO}(1 - 0)$ superbubble image (thin contour with grayscale map; Matsushita et al. 2000). The plus mark is the same as Fig. 1. The linear scale at M82 is shown in the bottom-right of the figure.